

Stimulated-emission cross section and fluorescent quantum efficiency of Nd^{3+} in yttrium aluminum garnet at room temperature

S. Singh, R. G. Smith, and L. G. Van Uitert

Bell Laboratories, Murray Hill, New Jersey 07974

(Received 31 January 1974)

The stimulated-emission cross sections and fluorescence branching ratios for the principal fluorescence transitions of YAG:Nd emanating from the ${}^4F_{3/2}$ state have been measured at room temperature. The peak cross section of the well-known 1064.2-nm laser line is here found to have a value of 4.6×10^{-19} cm^2 . Since the cross sections reported here are inconsistent with the generally accepted value of near unity for the radiative quantum efficiency η of the ${}^4F_{3/2}$ state the quantity η has been measured directly. A value of 0.56 ± 0.11 is found for η which is consistent with the observed fluorescence lifetime of the ${}^4F_{3/2}$ state and the measured cross sections.

I. INTRODUCTION

The stimulated-emission cross section σ is one of the important parameters in determining the threshold and efficiency for a given transition in a laser material. Since the first successful operation of the neodymium-doped yttrium aluminum garnet (YAG:Nd $^{3+}$) laser¹ there have been a number of experimental determinations²⁻⁷ of the cross section for the 1064.2-nm laser transition. The results reported by different investigators for the peak differential cross section of this particular transition have ranged from 2.7×10^{-19} to 8.8×10^{-19} cm^2 . Because of the wide variations between these reported values and the general usefulness of YAG:Nd $^{3+}$ as a standard with which to compare other Nd $^{3+}$ -doped laser materials, we have remeasured the cross sections of the various transitions in this material.

In this paper we report the results of our measurements of the stimulated-emission cross sections and fluorescence branching ratios for the principal fluorescence transitions of YAG:Nd $^{3+}$ emanating from the ${}^4F_{3/2}$ (*R* levels) state and terminating on the ${}^4I_{9/2}$ (*Z* levels), ${}^4I_{11/2}$ (*Y* levels), and ${}^4I_{13/2}$ (*X* levels) states⁸ at room temperature.

We obtain branching ratios in substantial agreement with those reported by Kushida *et al.*,³ but we find cross-section values which are approximately one-half those reported by Kushida *et al.*³ Since the cross sections reported here are inconsistent with the generally accepted value of near unity^{5,9} for the radiative quantum efficiency (η) of the ${}^4F_{3/2}$ state of Nd $^{3+}$ in crystals, we have directly measured the quantity η . We find a value of 0.56 ± 0.11 , which is consistent with the observed lifetime of the ${}^4F_{3/2}$ state and our measured cross sections.

II. MEASUREMENT TECHNIQUE

The following spectroscopic methods were used in determining the peak cross sections: (i) Direct measurement of the cross section in absorption. The Stark levels of the ${}^4I_{9/2}$ ground state are sufficiently populated at room temperature to determine the cross sections for the ${}^4F_{3/2} \rightarrow {}^4I_{9/2}$ transitions from the absorption data. Alves *et al.*⁴ have employed this method to measure the cross section of the 1064.2-nm fluorescence transition. Since the Boltzmann factor for the terminal level Y_3 of this transition, which is 2109 cm^{-1} above the ground level *Z*, is $\approx 6.8 \times 10^{-5}$ times that of the ground level, the accuracy with which direct absorption from this level can be measured is rather poor. Therefore, no attempt was made to measure σ 's for the ${}^4F_{3/2} \rightarrow {}^4I_{11/2, 13/2}$ transitions by this method. (ii) The cross section can be derived from the branching ratio, fluorescence decay time, and quantum efficiency of the fluorescing ${}^4F_{3/2}$ state. This technique relies crucially upon the knowledge of the quantum efficiency which, as is shown here, can not be assumed to be unity. (iii) The cross section of a given transition can be obtained by comparing the emission intensity associated with it with that of another emission line for which the cross section is already known from either of the above two methods. Most of the cross sections reported here were measured or checked using this method.

III. EXPERIMENTAL METHOD

Most of the measurements were made on a well-characterized piece of $\text{Y}_{2.97}\text{Nd}_{0.03}\text{Al}_5\text{O}_{12}$ having the dimensions $1.4 \times 1.36 \times 0.1875$ cm. The sample was kindly loaned to us by Dr. Geusic of our labora-

tory and was one of the specimens used by Kushida *et al.*³ who had a part of the boule chemically analyzed to establish its Nd concentration as 1 ± 0.01 at. % of the Y+Nd present. To check the concentration, a small portion of the sample was powdered and compared with a standard fused sample containing 1-at. % Nd using x-ray fluorescence. A true crystal concentration of 0.98 ± 0.02 -at. % Nd was found, in good agreement with the earlier chemical analysis. As is found in most Czochralski-grown crystals, there was a central core in the sample. For optical measurements, this core area was masked off.

Additional measurements of σ for the 1064.2-nm laser transition were made with another flux-grown sample of YAG:Nd³⁺. The Nd concentration in this sample was established to be 4 at. % by comparing the strength of its absorption lines with those in the 1-at. % Nd slab described above.

The fluorescence spectra were excited by either a pulsed argon-ion laser or a GaAsP light-emitting diode (LED), the latter emitting at 810 nm. The spectra were measured with a $\frac{3}{4}$ -m Spex monochromator with a 1200-grooves/mm grating blazed for 1.0 μm . A cooled 7102 photomultiplier served as a detector for the groups lying between 860 and 1150 nm, whereas a cooled PbS photodetector was employed for the 1.3- μm group. Both detectors were cooled to dry-ice temperature. Calibrated neutral density filters were used on the entrance slit of the spectrometer to ensure that the detectors were operated in their linear ranges only. Calibrated Corning glass filters were used to make certain that radiation in the desired spectral region only was measured. The detectors were calibrated against standard lamps both before and after each fluorescence run to ensure against changes in the relative wavelength sensitivity of the detectors due to any drift in the detector temperature. Absorption data on the samples studied were obtained with a Cary Model No. 14 spectrophotometer and independently with the Spex monochromator described above. Fluorescent-decay-time measurements were made using repetitive light pulses from the argon-ion laser or the LED and a 100-channel PAR waveform educator.

IV. BRANCHING RATIOS

When excited with either 514.5-nm or 810-nm radiation, fluorescence was observed in both samples from the R_1 and R_2 levels of the ${}^4F_{3/2}$ state to levels of the ${}^4I_{9/2}$, ${}^4I_{11/2}$, and ${}^4I_{13/2}$ states. However, no emission terminating on the ${}^4I_{15/2}$ state was observed. Also, no fluorescence could be detected from any other excited state lying higher

than the ${}^4F_{3/2}$ state. A partial energy level diagram of interest for YAG:Nd³⁺, based on our room-temperature absorption and fluorescence measurements, is shown in Fig. 1.

The fluorescence spectra were excited from both the front and back surfaces of the crystal. Reabsorption of fluorescence, particularly important for transitions from the ${}^4F_{3/2}$ to the ${}^4I_{9/2}$ levels, was corrected for by the following formulae¹⁰: For front face excitation the observed emission was multiplied by a factor F_R , given by

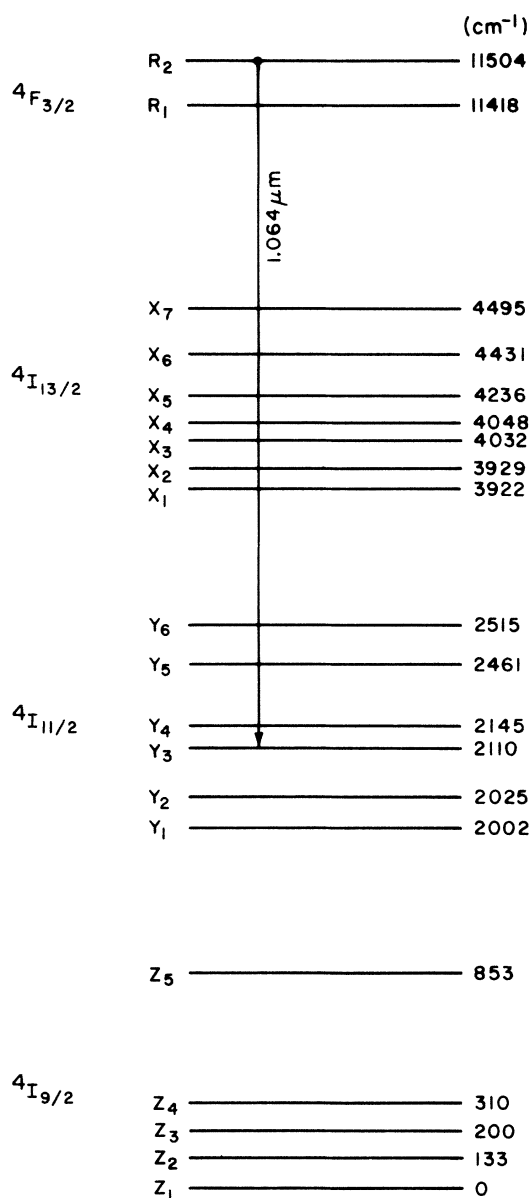


FIG. 1. Partial energy level diagram of the low-lying levels of Nd³⁺ in YAG.

$$F_R = \frac{1 - \exp(-\alpha_p L)}{1 - \exp[-(\alpha_p + \alpha_f)L]} \frac{\alpha_p + \alpha_f}{\alpha_p}, \quad (1)$$

where α_p is the absorption coefficient at the pump wavelength, α_f is the absorption coefficient at the fluorescence wavelength, and L is the thickness of the specimen along the direction of observation. The correction factor F_T for fluorescence excited from the rear face (in transmission) is given by

$$F_T = \frac{1 - \exp(-\alpha_p L)}{\exp(-\alpha_f L) - \exp(-\alpha_p L)} \frac{\alpha_p - \alpha_f}{\alpha_p} \quad (2)$$

The branching ratio as used here is defined on a photon basis as the fraction of the total fluorescence going into a given transition. The fluorescence branching ratio of the j th emission line, β_j , is thus given by

$$\beta_j = \frac{\text{Number of photons radiated into } j\text{th emission line}}{\text{Total number of photons radiated}} = \frac{\int \lambda I_j(\lambda) d\lambda}{\sum_j \int \lambda I_j(\lambda) d\lambda}, \quad (3)$$

where $I_j(\lambda)$ is the radiated power per unit wavelength interval associated with the j th emission line. In determining the β_j a standard lamp of known spectral distribution was used in calibrating the emission power from each line. The integrals were determined using a planimeter as well as by

TABLE I. Branching ratios and stimulated-emission cross sections of the observed fluorescence transitions in YAG: Nd³⁺ at room temperature.

λ (nm)	ν (cm ⁻¹)	Transition	$\Delta\nu$ (cm ⁻¹)	σ (10 ⁻²⁰ cm ²)	β
869.0	11504	$R_2 \rightarrow Z_1$	13	4.2	0.033
875.4	11420	$R_1 \rightarrow Z_1$	10	1.1	0.013
879.2	113719	$R_2 \rightarrow Z_2$	18	1.3	0.017
884.4	11304	$R_2 \rightarrow Z_3$	19	4.2	0.036
885.8	11286	$R_1 \rightarrow Z_2$	19	3.5	0.066
891.1	11219	$R_1 \rightarrow Z_3$	10	2.4	0.040
893.4	11190	$R_2 \rightarrow Z_4$	31	0.5	0.004
900.0	11108	$R_1 \rightarrow Z_4$	31	1.2	0.037
938.6	10651	$R_2 \rightarrow Z_5$	10	4.8	0.030
946.1	10567	$R_1 \rightarrow Z_5$	9	5.1	0.040
1052.13	9502	$R_2 \rightarrow Y_1$	5	15.1	0.042
1055.05	9475	$R_2 \rightarrow Y_2$	5	1.1	0.006
1061.58	9422	$R_1 \rightarrow Y_1$	4	22.8	0.079
1064.18	9394	$R_2 \rightarrow Y_3$	5	45.8	0.135
1064.55	9391	$R_1 \rightarrow Y_2$	5	8.1	0.030
1068.26	9358	$R_2 \rightarrow Y_4$	10	6.7	0.036
1073.85	9310	$R_1 \rightarrow Y_3$	4	16.3	0.061
1078.0	9274	$R_1 \rightarrow Y_4$	9	4.6	0.045
1105.42	9044	$R_2 \rightarrow Y_5$	20	2.0	0.02
1112.12	8989	$R_2 \rightarrow Y_6$	14	3.6	0.025
1115.95	8959	$R_1 \rightarrow Y_5$	16	2.9	0.034
1122.7	8905	$R_1 \rightarrow Y_6$	13	3.0	0.030
1318.8	7581	$R_2 X_1$	6	8.7	0.018
1320.0	7574	$R_2 X_2$	6	1.9	0.004
1333.8	7495	$R_1 X_1$	6	3.0	0.009
1335.0	7489	$R_1 X_2$	6	3.4	0.009
1338.2	7471	$R_2 X_3$	6	9.2	0.021
1341.0	7455	$R_2 X_4$	9	3.5	0.011
1353.6	7386	$R_1 X_3$	7	1.4	0.005
1356.4	7370	$R_1 X_4$	8	4.4	0.0175
1414.0	7070	$R_2 X_6$	15	3.3	0.016
1430.8	6987	$R_1 X_6$	15	2.3	0.0145
1444.0	6923	$R_1 X_7$	10	3.4	0.0162

assuming a Lorentzian line shape and using the peak emission intensities and linewidth with essentially identical results. The branching ratios for all lines observed in emission are listed in the last column of Table I. The individual branching ratios are accurate to $\pm 15\%$. The total branching ratios for the various manifolds are summarized in Table II along with those previously reported by Kushida *et al.*³ and more recently by Watts.¹¹ To be consistent, the branching ratios of Ref. 11—where β was defined in terms of the fluorescent power rather than quanta—have been converted to the photon basis used here. Within experimental accuracy there is reasonable agreement between our data and those of Ref. 3. Our results are in exact agreement with those predicted by Krupke.¹² However, the total branching ratio of the ${}^4F_{3/2} \rightarrow {}^4I_{9/2}$ transition reported in Ref. 10 is considerably lower than our value. The lower value could be accounted for if the author of Ref. 10 neglected the correction for self-absorption which is important for the ${}^4F_{3/2} \rightarrow {}^4I_{9/2}$ transitions.

V. CROSS SECTIONS

Since the total crystal-field splitting of the ground state ${}^4I_{9/2}$ is only $\sim 4kT$ (853 cm⁻¹) all of its Stark levels are thermally populated at room temperature. Therefore, reasonable amounts of absorption could be observed from each of the five levels of ${}^4I_{9/2}$ to the two levels of ${}^4F_{3/2}$. The peak absorption cross sections for the ${}^4F_{3/2} \rightarrow {}^4I_{9/2}$

TABLE II. Branching ratios for transitions ${}^4F_{3/2} \rightarrow {}^4I_J$ multiplets of YAG: Nd³⁺ at 300°K.

Transition	λ (nm)	β		
		Present work	Ref. 3	Ref. 11
${}^4F_{3/2} \rightarrow {}^4I_{9/2}$	865–950	0.32	0.25	0.20
${}^4F_{3/2} \rightarrow {}^4I_{11/2}$	1050–1130	0.54	0.60	0.65
${}^4F_{3/2} \rightarrow {}^4I_{13/2}$	1317–1450	0.14	0.15	0.15

transitions were determined from the absorption data by using the relation

$$\sigma = \alpha / N_i, \quad (4)$$

where α is the peak absorption coefficient and N_i is the population density of the Nd^{3+} ions in the lower initial level from which absorption takes place. The observed peak absorption cross sections are summarized in Table III. The values obtained for the $R_1 \rightarrow Z_1$ and $R_2 \rightarrow Z_1$ transitions are 1.1×10^{-20} and 4.2×10^{-20} cm^2 , respectively, and are in excellent agreement with those obtained by Kushida and co-workers,³ who report values of 1.1×10^{-20} cm^2 and 4.1×10^{-20} cm^2 .

The peak differential cross sections for the various transitions emanating from the ${}^4F_{3/2}$ state were determined by comparing the fluorescence intensity of the line in question to that of a line whose cross section is known from absorption measurements. The relation between the cross sections of two lines emanating from the same upper-level u but terminating on lower levels l and g , respectively, is

$$\frac{\sigma_{ug}}{\sigma_{ul}} = \left(\frac{n_{ul}}{n_{ug}} \right)^2 \left(\frac{\nu_{ul}}{\nu_{ug}} \right)^3 \left[\left(\frac{dI}{d\nu} \right)_{ug} / \left(\frac{dI}{d\nu} \right)_{ul} \right], \quad (5)$$

where $dI/d\nu$ is the peak emission power per unit frequency interval, ν is the emission frequency, and n is the refractive index. When expressed in terms of the more directly measured power per unit wavelength interval, the above expression becomes

$$\frac{\sigma_{ug}}{\sigma_{ul}} = \left(\frac{n_{ul}}{n_{ug}} \right)^2 \left(\frac{\lambda_{ug}}{\lambda_{ul}} \right)^5 \left[\left(\frac{dI}{d\lambda} \right)_{ug} / \left(\frac{dI}{d\lambda} \right)_{ul} \right], \quad (6)$$

where λ is the vacuum wavelength. In these expressions the degeneracy factors cancel out because each of the levels of Nd^{3+} is a Kramers doublet. If the two transitions terminating on

levels l and g originate from two different upper levels which are in thermal equilibrium with each other, then Eq. (6) is modified by the appropriate Boltzmann factor. The peak emission cross section of a given line contained in the transitions ${}^4F_{3/2} \rightarrow {}^4I_{9/2, 11/2, 13/2}$ was determined by comparing its emission with the following lines: 869.0, 875.4, 900.0, 938.6, and 946.1 nm, all of which terminate on the Z levels and are relatively free of other overlapping lines. The peak cross sections obtained in this manner are summarized in the fourth column of Table I. The accuracy of these measurements is $\pm 15\%$.

In comparing these results with those of Kushida *et al.*³ it is found that all inferred cross sections are smaller by approximately a factor of 2. In particular the cross section of the dominant 1064.2-nm emission line ($R_2 \rightarrow Y_3$) is here found to have a peak differential cross section of 4.6×10^{-19} cm^2 compared to a value of 8.0×10^{-19} cm^2 .³ The peak cross section of the laser emission, composed of the partially overlapping $R_2 \rightarrow Y_3$ and $R_1 \rightarrow Y_2$ lines, is here found to be $\sim 5 \times 10^{-19}$ cm^2 as compared with a value of 8.8×10^{-19} cm^2 determined by the authors of Ref. 3. This value of the cross section is also to be compared with values of 2.7×10^{-19} and 3.5×10^{-19} cm^2 reported by Neeland and Evtuhov,² 5.6×10^{-19} cm^2 by Alves *et al.*,⁴ 7×10^{-19} cm^2 by Weber and Varitimos,⁵ 8.8×10^{-19} cm^2 by Birnbaum and Gelwachs,⁶ and 7.2×10^{-19} cm^2 by Vanderleeden and Szabo.⁷

The inconsistencies between the values reported here and those reported elsewhere far exceed the estimated errors. As a possible check on our measured cross sections, the total radiative lifetime T_r of the ${}^4F_{3/2}$ state was computed from the relation

$$T_r = \lambda^2 \beta / 4\pi^2 n^2 \sigma \Delta \nu F, \quad (7)$$

TABLE III. Peak absorption cross sections for the lines of the ${}^4F_{3/2} \rightarrow {}^4I_{9/2}$ transition in $\text{Y}_{2.97}\text{Nd}_{0.03}\text{Al}_5\text{O}_{12}$ at 300 °K.

Wavelength (nm)	Transition	Nd^{3+} density in initial level (cm^{-3})	Peak α (cm^{-1})	Peak σ (10^{-20} cm^2)
869.0	$R_2 \rightarrow Z_1$	6.45×10^{19}	2.7	4.2
875.4	$R_1 \rightarrow Z_1$	6.45×10^{19}	0.7	1.1
879.2	$R_2 \rightarrow Z_2$	3.41×10^{19}	0.4	1.2
884.4	$R_2 \rightarrow Z_3$	2.47×10^{19}	1.27	5.1
885.8	$R_1 \rightarrow Z_2$	3.41×10^{19}	1.3	3.8
891.1	$R_1 \rightarrow Z_3$	2.47×10^{19}	0.58	2.3
900.0	$R_1 \rightarrow Z_4$	1.46×10^{19}	0.16	1.1
938.6	$R_2 \rightarrow Z_5$	1.08×10^{18}	0.05	4.5
946.1	$R_1 \rightarrow Z_5$	1.08×10^{18}	0.05	4.8

where λ is the vacuum wavelength of emission, $\Delta\nu$ is the full width at half-maximum of the emission line, β is the branching ratio, n is the refractive index, σ is the cross section, and F is the fraction of ions in the emitting level which has the values 0.60 and 0.40 for the R_1 and R_2 levels, respectively. Using our measured values for the above quantities we determine $T_r(^4F_{3/2}) = 411 \mu\text{sec}$. This value for the radiative lifetime taken along with the measured fluorescence lifetime $T_f = 230 \mu\text{sec}$ implies a radiative quantum efficiency $\eta = T_f/T_r = 0.56$, which is considerably less than the value of 0.995 inferred by Kushida *et al.* in their optical refrigeration experiment.⁹ In order to attempt to resolve the question of quantum efficiency and to determine the cross section independently from branching ratio, fluorescence lifetime, linewidth, and quantum efficiency, the quantum efficiency of the material studied was measured as described in the Sec. VI.

VI. QUANTUM EFFICIENCY

In order to determine the fluorescence quantum efficiency of the upper state—in this case the $^4F_{3/2}$ state—it is necessary to know the amount of pump power absorbed by the sample and the total amount of fluorescence radiation. The following procedure, which is quite straightforward and in need of fewer corrections than the one utilizing an integrating sphere, was used. The experimental setup is shown in Fig. 2. The detection system was similar to that described previously except as discussed below.

The fluorescence of the YAG:Nd³⁺ sample was excited by the pulsed argon laser. The multiwavelength output of the laser was passed through a $\frac{1}{4}$ -m Bausch & Lomb monochromator and the

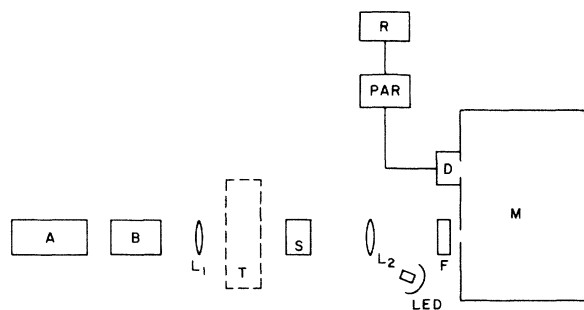


FIG. 2. Block diagram of the experimental arrangement used for measurements of fluorescent quantum efficiency, branching ratio, and stimulated-emission cross section. A, argon laser; B, Bausch & Lomb $\frac{1}{4}$ -m monochromator; L_1 , lens of $f=10$ cm; T, GaAsP light-emitting diode housed in an ellipse; M, Spex monochromator; D, detector; PAR, lock-in amplifier or an electrometer; and R, strip chart recorder.

514.5-nm line was isolated. The pumping radiation was focused into the sample collinearly with the direction of observation and with a spot size small compared with the image of the entrance slit as seen through the collecting lens L_2 . The incident pump power at 514.5 nm was measured with an Eppley thermopile. The amount of power absorbed by the sample was obtained from the relation

$$P_{\text{abs}} = P_0(1 - e^{-\alpha_p L}), \quad (8)$$

where P_0 is the net incident power into the sample after correction for reflection losses, L is the thickness of the sample, and α_p is the absorption coefficient, which was determined to be 0.43 cm^{-1} by measurements with the spectrophotometer. The sample was placed so that the illuminated volume was imaged on the plane of the entrance slit of the spectrometer. The entrance slit opening was such that the image of the illuminated spot fell fully within the slit opening. The exit slit was then opened to the point where the fluorescence signal no longer increased. This procedure ensured that the spectrometer collected all of the fluorescent radiation emitted by the sample volume contained within the solid angle subtended by the collecting lens L_2 . The fluorescence signal was then recorded.

The system was calibrated by removing the YAG:Nd³⁺ sample and replacing it with a ribbon-filament spectral-radiance standard lamp. The lamp filament was carefully placed the same distance from the spectrometer. The lens, slits, and other apparatus were left unchanged. Calibrated filters were then inserted to attenuate the calibrating signal to the same general level as the fluorescence, and the calibration was recorded. In order to complete the calibration it is necessary to know further the transmission characteristic of the spectrometer and the effective area of the ribbon filament seen by the spectrometer. The former was measured by using a He-Ne laser at 1152 nm to determine the spectrometer response, which was found to be trapezoidal in shape, as expected for unequal slit widths. Corrections were made in converting the slit function to other wavelengths. The effective area of the filament lamp was determined by illuminating the exit slit of the spectrometer with a tungsten lamp and measuring the width and height of the image of the entrance slit at the sample plane. The latter measurements were made with a traveling microscope. As mentioned above, in exciting the fluorescence the volume of the sample illuminated by the argon pump beam was made to fall within the acceptance region of the spectrometer.

In determining the calibration of the system

only the solid angle of acceptance is unknown. Since the solid angle is the same—after correcting for the refractive index of YAG—for both the calibration and fluorescence measurements it drops out in determining the quantum efficiency.

The above procedure was applied for a number of the fluorescence lines of the sample. The fluorescent quantum efficiency η of the emitting state (${}^4F_{3/2}$) is defined as

$$\eta = q_f/q_a, \quad (9)$$

where q_f is the total number of fluorescent quanta per second emitted in all of the transitions emanating from the emitting state and q_a is the number of photons absorbed per second. The latter quantity was determined from $P_{\text{abs}}/h\nu_p$, where ν_p is the pump frequency and h is Planck's constant, and the previously established¹³ value of unity for the radiationless transfer from the pump level (${}^2G_{7/2}$) to the ${}^4F_{3/2}$ state has been assumed. The total number of fluorescence quanta emitted per second was obtained from the relation

$$q_f = \frac{4\pi n^2 A \lambda \Delta \lambda}{\beta h c} \frac{r_f}{r_s} \frac{dE}{d\lambda}, \quad (10)$$

where λ is the fluorescence wavelength, A is the effective area of the standard lamp filament imaged on the entrance slit, $\Delta \lambda$ is the exit slit width required to transmit essentially all of the fluorescence radiation, β is the branching ratio, r_f and r_s are the detector responses for the fluorescence and standard lamp radiation, respectively, $dE/d\lambda$ is the spectral irradiance of the standard lamp, n is the refractive index, h is Planck's constant and c is the velocity of light. The results are summarized in Table IV. The values of the quantum efficiency so determined vary from a low of 0.5 to a high of 0.63, with an average value of 0.56.

The accuracy of the quantum efficiency as determined in this way is critically dependent upon a number of factors, not the least of which is the absolute calibration of the Eppley thermopile. The effective area of the lampblack surface of the thermopile was determined by measuring its optimum output for radiation from a tungsten lamp passing through a series of apertures of known openings. The accuracy of this measurement is estimated to be $\pm 20\%$. The important aspect of the measurement is that it confirms with reasonable certainty the implications of Sec. V that the quantum efficiency deviates significantly from unity. The agreement between the quantum efficiency determined here (0.56) and that inferred from the radiative and fluorescent lifetimes (0.565) is better than could be expected considering the associated uncertainties. Whereas a knowledge of

quantum efficiency, lifetime, linewidth, and branching ratio suffices to determine cross sections, the method employed previously is certainly the preferred method.

VII. DISCUSSION

The principal result of this work is the re-determination of the cross sections of the transitions from the ${}^4F_{3/2}$ level of Nd^{3+} in YAG. The values determined for those transitions not observed directly in absorption are smaller than those determined by Kushida *et al.*³ and, in particular, the peak cross section of the important 1064-nm laser transition is smaller by roughly a factor of 2 than the widely accepted value,³ $5 \times 10^{-19} \text{ cm}^2$ vs $8.8 \times 10^{-19} \text{ cm}^2$. The implication of this result is that the fluorescent quantum efficiency is less than unity; measurements of the quantum efficiency made here agree with the value calculated from lifetime, linewidths, and cross sections.

Since these results are in disagreement with the results of Kushida *et al.*, it is important to ask if the nonradiative paths from the ${}^4F_{3/2}$ state could be sufficiently fast to cause the decreased quantum efficiency. The nonradiative lifetime T_{nr} is related to the fluorescence lifetime T_f and quantum efficiency as

$$1/T_f = \eta/T_f + 1/T_{\text{nr}}. \quad (11)$$

The nonradiative lifetime consistent with the measured fluorescent lifetime of 230 μsec and $\eta = 0.56$ is 522 μsec .

Nonradiative relaxation between electronic states of rare-earth ions in solids can occur via the emission or absorption of phonons. The magnitude of the multiphonon transition rate depends upon the phonon frequency distribution in the host lattice. It has been established by Hurrell *et al.*¹⁴ from measurements on infrared reflectivity and

TABLE IV. Radiative quantum efficiency of ${}^4F_{3/2}$ state of YAG:Nd at room temperature.

λ (nm)	Transition	β	η
869.0	$R_2 \rightarrow Z_1$	0.0325	0.53
875.4	$R_1 \rightarrow Z_1$	0.0133	0.57
900.0	$F_1 \rightarrow Z_4$	0.0365	0.50
938.6	$R_2 \rightarrow Z_5$	0.0295	0.59
946.1	$R_1 \rightarrow Z_5$	0.04	0.62
1052.1	$R_2 \rightarrow Y_1$	0.042	0.54
1061.6	$R_1 \rightarrow Y_1$	0.079	0.53
1064.2	$\left[\begin{array}{l} R_2 \rightarrow Y_3 \\ R_1 \rightarrow Y_2 \end{array} \right]$	0.165	0.63
1073.8	$R_1 \rightarrow Y_3$	0.061	0.55
1078.0	$R_1 \rightarrow Y_4$	0.045	0.58

Raman spectra that phonons of frequencies up to $\sim 857 \text{ cm}^{-1}$ are present in YAG. Zverev *et al.*¹⁵ have concluded from the vibronic spectra of YAG:Nd that the most strongly coupled phonons are those with frequency $\sim 700 \text{ cm}^{-1}$. In YAG:Nd the R_1 level of ${}^4F_{3/2}$ is separated by $\sim 4660 \text{ cm}^{-1}$ from the nearest level (W_3) of ${}^4I_{15/2}$ state. Therefore, a total of approximately seven phonons would be required for a nonradiative relaxation ${}^4F_{3/2} \rightarrow {}^4I_{15/2}$. Zverev *et al.*¹⁵ have estimated from their measurements of the fluorescent lifetime of the ${}^4F_{3/2}$ state in YAG:0.5-at. % Nd as a function of temperature that the transition rate for the nonradiative relaxation ${}^4F_{3/2} \rightarrow {}^4I_{15/2}$ is $\sim 10^2 \text{ sec}^{-1}$. This result when used in Eq. (11) predicts a radiative lifetime $T_r \sim 250 \mu\text{sec}$, which in turn implies a radiative quantum efficiency $\eta \sim 1$. It should be pointed out that such a conclusion is based upon the assumption that the ${}^4F_{3/2}$ state relaxes nonradiatively only via a multiphonon process. However, since a ${}^4F_{3/2} \rightarrow {}^4I_{15/2}$ transition in YAG:Nd³⁺ perfectly matches a ${}^4I_{15/2} \rightarrow {}^4I_{9/2}$ transition, quenching via multipolar transfer as well as by resonant transfer eventually dumping into an impurity or lattice defect are both possible. Since we measure a radiative quantum efficiency of less than unity and also have evidence¹⁶ of much higher fluorescent lifetimes at low Nd concentrations, we can only conclude that such paths for nonradiative decay are operative in YAG:Nd³⁺

VIII. CONCLUSION

We have measured the branching ratios, radiative quantum efficiency, and stimulated emission cross sections for the various fluorescent transitions in Nd³⁺-doped Y₃Al₅O₁₂ crystals. The branching ratios are in reasonable agreement with those of earlier workers. The absolute quantum efficiency of the ${}^4F_{3/2}$ metastable state is found to be 0.56 compared with the widely used value of unity which would result in a lower overall efficiency of the YAG:Nd³⁺ laser. The emission cross section for the well-known 1064.2-nm laser line is found to be $5 \times 10^{-19} \text{ cm}^2$ at room temperature, which is about half of the widely accepted value of $8.8 \times 10^{-19} \text{ cm}^2$. The implication of a lower cross section is a higher theoretical value for the cw laser threshold for a given loss.

ACKNOWLEDGMENTS

It is a pleasure to thank M. DiDomenico, Jr. for suggesting to undertake the work presented here and his many other valuable suggestions during its course. The excellent technical assistance of J. R. Potopowicz is greatly appreciated. Thanks are due to Miss B. Prescott for data on transmission in the samples.

¹J. E. Geusic, H. M. Marcos, and L. G. Van Uitert, *Appl. Phys. Lett.* **4**, 182 (1964).

²J. K. Neeland and V. Evtuhov, *Phys. Rev.* **156**, 244 (1967).

³T. Kushida, H. M. Marcos, and J. E. Geusic, *Phys. Rev.* **167**, 289 (1968).

⁴R. V. Alves, R. A. Buchanan, K. A. Wickersheim, and E. A. C. Yates, *J. Appl. Phys.* **42**, 3043 (1971).

⁵M. J. Weber and T. E. Varitimos, *J. Appl. Phys.* **42**, 4996 (1971).

⁶M. Birnbaum and J. A. Gelwachs, *J. Appl. Phys.* **43**, 2335 (1972).

⁷J. C. Vanderleeden and T. Szabo (private communication).

⁸In labeling the Stark levels of the various states of Nd³⁺, we have followed the nomenclature used in G. H. Dieke, *Spectra and Energy Levels of Rare-Earth Ions in Crystals* (Interscience, New York, 1968).

als (Interscience, New York, 1968).

⁹T. Kushida and J. E. Geusic, *Phys. Rev. Lett.* **21**, 1172 (1968).

¹⁰N. K. Chaudhury, *Z. Phys.* **151**, 93 (1958).

¹¹R. K. Watts, *J. Opt. Soc. Am.* **61**, 123 (1971).

¹²W. F. Krupke, *IEEE J. Quantum Electron.* **QE-7**, 153 (1971).

¹³R. A. Brandewie and C. L. Telk, *J. Opt. Soc. Am.* **57**, 1221 (1967).

¹⁴J. P. Hurrell, S. P. S. Porto, I. F. Chang, S. S. Mitra, and P. P. Bawras, *Phys. Rev.* **173**, 851 (1968).

¹⁵G. M. Zverev, G. Ya. Kolodny, and A. M. Onishchenko, *Zh. Eksp. Teor. Fiz.* **60**, 920 (1971) [*Sov. Phys.-JETP* **33**, 497 (1971)].

¹⁶S. Singh, W. A. Bonner, L. G. Van Uitert, and G. Zydzić (unpublished).